

# Geometry effects in topologically confined bilayer graphene loops

Nassima Bachtaber,<sup>1</sup> David Sánchez,<sup>1,2</sup> and Llorenç Serra<sup>1,2</sup>

<sup>1</sup>*Institute of Interdisciplinary Physics and Complex Systems IFISC (CSIC-UIB), E-07122 Palma, Spain*

<sup>2</sup>*Department of Physics, University of the Balearic Islands, E-07122 Palma, Spain*

We investigate the electronic confinement in bilayer graphene by topological loops of different shapes. These loops are created by lateral gates acting via gap inversion on the two graphene sheets. For large-area loops the spectrum is well described by a quantization rule depending only on the loop perimeter. For small sizes, the spectrum depends on the loop shape. We find that zero-energy states exhibit a characteristic pattern that strongly depends on the spatial symmetry. We show this by considering loops of higher to lower symmetry (circle, square, rectangle and irregular polygon). Interestingly, magnetic field causes valley splittings of the states, an asymmetry between energy reversal states, flux periodicities and the emergence of persistent currents.

## I. INTRODUCTION

One of the most fundamental predictions of Quantum Mechanics is the existence of confined or bound states which are eigenstates of the Hamiltonian describing a particular system<sup>1</sup>. It is well known that the Schrödinger equation with a spatially dependent potential yields in many cases bound eigenstates located around the absolute potential minima. This potential binding mechanism around minima is crucial in many natural physical systems like, e.g., electrons in atoms and molecules<sup>2</sup>; and it is also behind the formation of artificial bound states by potential gating with microelectrodes, as in semiconductor quantum dots<sup>3</sup>. In bilayer graphene (BLG) with Bernal stacking, the material we consider in this work, a similar potential confinement mechanism exists but it is related to the potential difference  $V_a$  applied to split dual gates on the two graphene sheets; electrons are bound to the regions where  $V_a$  is lowest. These regions of lowest  $V_a$  can take different shapes, such as circular dots and rings for instance, and they have been intensively studied both theoretically and experimentally<sup>4-16</sup>. The technological interest of BLG nanostructures is twofold. First, they could serve as scalable spin qubits with long decoherence times due to the weak spin-orbit interaction in graphene<sup>17-19</sup>. Second, in combination with magnetic fields they could be utilized for valleytronic operations thanks to the manipulation of the valley degree of freedom<sup>20-22</sup>.

The possibility of an even more robust type of confinement in BLG was suggested in Ref. 23. This is a qualitatively different confinement, of a topological character, emerging near the domain wall that separates two regions where  $V_a$  changes sign. The confined states are intrinsically 1D-like, with a characteristic transverse decay length, and they propagate along the domain wall with locked relative orientations of momentum and valley pseudospin. In the absence of valley mixing potentials states for the K and K' valleys propagate along the wall, without backscattering, showing opposite chiralities. This property is similar to the helical states within the quantum spin Hall effect<sup>24-26</sup> if we replace spin with the valley pseudospin of graphene.

Now, let us suppose that the external gates are arranged in such a way that the domain wall closes into itself. A schematic representation is shown in Fig. 1a. Then, a loop forms supporting electronic bound states<sup>27</sup> and the following question naturally arises. What is the effect of different loop shapes onto the energy spectrum of these bound states? Being 1D-like, topologically confined states in BLG are expected to essentially depend on the loop perimeter unlike the trivial potential confinement, which depends both on the surface and the shape of the confining region. Nevertheless, it is important to notice that the domain-wall states depicted with a red line in Fig. 1a are in reality quasi-1D with a finite spatial width. Therefore, the discrete energy spectrum will be in general a function of the system's geometrical symmetries, the region aspect ratio, etc. Below, we present a detailed investigation for topological loops of different shapes and symmetries. First, we show with the aid of an exactly solvable model that the energy spectrum is uniquely determined by the loop perimeter provided that the system size is large. Yet, for smaller loops finite size effects become important and the spectrum depends on the particular geometrical structure. This dependence is better seen in the sequence of zero energy crossing and anticrossings as the perimeter increases.

In presence of a magnetic field  $B$ , the dispersion is affected by the flux piercing the topological loop. This creates an energy splitting for the two valleys and an asymmetry with respect to energy inversion ( $E \rightarrow -E$ ) in the spectra as a function of perimeter. The  $B$ -dependence of the spectra with a fixed perimeter and shape is characterized by magnetic periodicities of Aharonov-Bohm type. Therefore, the loops host persistent currents at finite fields that, similarly to the  $B = 0$  spectra, exhibit geometry dependent features in the small size limit, showing that currents would serve as an excellent tool to probe topologically confined states in BLG nanostructures.

## II. THEORY

### A. A Quantized-perimeter model (QPM)

An analytic model of topological loops in BLG can be devised utilizing the results of Ref. 23 for a straight domain wall with an abrupt transition  $+V_a$  to  $-V_a$  (a kink). The analytic relations between linear momentum  $p$  along the kink and energy  $E$  of the two topological branches, corresponding to the two valleys ( $K, K'$ ), were given in Ref. 23 as  $p = f_{1,2}(E)$ , with

$$f_{1,2}(E) = \frac{-E \pm \frac{V_a}{\sqrt{2}}}{(\mp E + V_a \sqrt{2})^{1/2}} \frac{\sqrt{t}}{\sqrt{2}v_F}, \quad (1)$$

where the Fermi velocity  $\hbar v_F = 660 \text{ meV nm}$  and the interlayer coupling  $t = 380 \text{ meV}$  are BLG intrinsic parameters.

In a closed loop of perimeter  $\mathcal{P}$  we can assume that the tangent momentum  $p$  is quantized, such that an integer number of wavelengths must fit into  $\mathcal{P}$ ,

$$p \rightarrow p_n \equiv \hbar \frac{2\pi n}{\mathcal{P}}, \quad n = \pm 1, \pm 2, \dots, \quad (2)$$

where negatives  $n$ 's represent negative momenta (i.e., opposite propagation) and the perimeter quantization in terms of wavelength  $\lambda$  reads  $\mathcal{P} = |n|\lambda$ . We can also add a magnetic field, represented by a vector potential  $\vec{A}$ , and

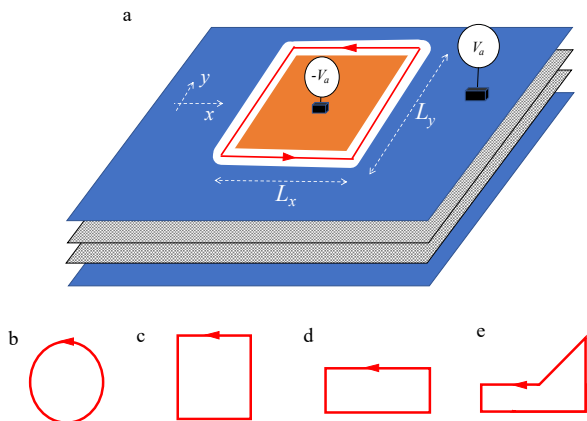


FIG. 1. a) Scheme of a topological loop showing the bilayer graphene sheets (gray) and lateral gates with the applied gate potentials  $\pm V_a$  (orange and blue, respectively). Two identical lower gates, hidden behind the lower graphene sheet, have the opposite potentials of the corresponding top gates. The white 1D region between orange and blue gates hosts the topological loop state on the graphene sheets, with counterpropagation for the two valleys. A red arrow is indicating the circulation for only one of the two valleys. b)-e) Loop shapes considered in this work, from highest to lowest symmetry: circle, square, rectangle and irregular polygon.

write the circulation integral

$$\int_{\mathcal{P}} dl (p_n + eA_t) = f_{1,2}(E) \int_{\mathcal{P}} dl, \quad (3)$$

where  $A_t$  is the component of the vector potential tangent to the kink. Noticing that  $\int_{\mathcal{P}} dl = \mathcal{P}$  and  $\int_{\mathcal{P}} dl A_t = \Phi$ ,  $\Phi$  being the magnetic flux across the loop, we find an implicit condition from which one can derive the bound state energy  $E$  for a given loop perimeter, magnetic flux and principal quantum number  $n$ :

$$f_{1,2}(E) = \frac{2\pi\hbar}{\mathcal{P}} \left( \frac{\Phi}{\Phi_0} + n \right), \quad (4)$$

where  $\Phi_0 = h/e$  is the flux quantum.

Equation (4) is our quantized-perimeter model (QPM) for bound states in BLG topological loops. As anticipated, when  $\Phi = 0$  the relation depends only on the perimeter and is totally independent of the loop geometry. At finite fields, however, the bound-state energies depend on the loop surface through the Aharonov-Bohm flux ratio  $\Phi/\Phi_0$ . We expect the QPM to be reliable for large enough loops, when different parts of the loop do not interfere. In small loops, the traversal extension of the topological states becomes comparable to the distances inside the loop and the QPM breaks down. Below, we investigate deviations from the QPM using an exact approach for BLG within the continuum limit.

### B. A quantum 2D model (Q2DM)

The low-energy Hamiltonian describing the states that are formed in two-dimensional (2D) BLG nanostructures for energies near the Dirac points reads<sup>28,29</sup>

$$H = v_F \left( p_x - \hbar \frac{y}{l_z^2} \right) \tau_z \sigma_x + v_F p_y \sigma_y + \frac{t}{2} (\lambda_x \sigma_x + \lambda_y \sigma_y) + V_a(x, y) \lambda_z, \quad (5)$$

where  $\sigma_{x,y,z}$ ,  $\tau_{x,y,z}$  and  $\lambda_{x,y,z}$  are Pauli matrices for the sublattice, valley and layer pseudo spins, respectively. A topological loop forms from a space dependent function  $V_a(x, y)$  that, as sketched in Fig. 1a, takes the constant values  $+V_a$  ( $-V_a$ ) outside (inside) the loop. In our numerical simulations, we consider a smooth spatial transition with a diffusivity<sup>30</sup>  $s$  to mimic a realistic experiment<sup>31,32</sup>. Details of how we model the closed loops of different shapes are given in the Appendix. Finally, the field strength is included in the magnetic length  $l_z = \sqrt{\hbar/eB}$ .

We numerically look for the eigenstates of the Hamiltonian given by Eq. (5) using finite difference discretization of the  $xy$  plane in a square grid<sup>33</sup>. The spurious solutions due to Fermion doubling<sup>34-36</sup> have been filtered out as in Ref. 30 by coarse graining the wave functions. Our method can handle any symmetry of the loop, in contrast to radial grids which are of smaller dimension and

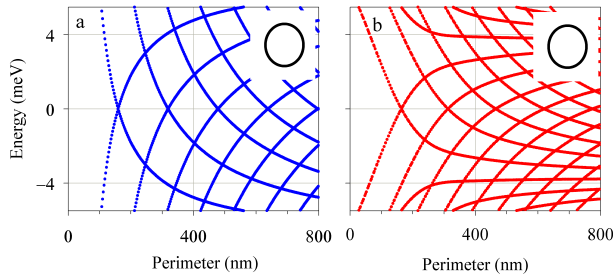


FIG. 2. QPM (a) and Q2DM (b) energy spectrum for a circle as a function of its perimeter at zero magnetic field. Parameters: wall potential  $V_a = 10$  meV and smoothness  $s = 12.5$  nm.

more efficient computationally, but can only describe radially symmetric structures by construction. In all the cases treated below we have checked that good convergence with the grid size is reached.

The Hamiltonian Eq. (5) fulfills a chiral symmetry given by operator  $\mathcal{C} = \sigma_x \tau_x \lambda_y$  relating eigenstates of opposite energies  $\mathcal{C}H\mathcal{C} = -H$  with  $\mathcal{C}^2 = 1$ . In absence of magnetic field it also fulfills time reversal symmetry  $\Theta = i\tau_y \mathcal{K}$ , with  $\mathcal{K}$  representing complex conjugation, relating states of the same energy  $\Theta H \Theta = -H$  and with  $\Theta^2 = -1$ .

### III. RESULTS

Figure 2 compares the bound state energies in the analytical (QPM) and numerical (Q2DM) approaches as a function of the loop perimeter when the structure is a circle. Qualitatively, both approaches nicely agree. At zero energy, the QPM predicts a sequence of uniformly spaced branch crossings, with spacing given by the zero-energy wavelength

$$\lambda_0 = 2^{5/4} \frac{2\pi \hbar v_F}{\sqrt{V_a t}}, \quad (6)$$

which for  $V_a = 10$  meV yields  $\lambda_0 \simeq 160$  nm. We then find an excellent correspondence with the zero energy crossings obtained numerically in the Q2DM. Physically, each branch corresponds to an angular momentum and, therefore, can produce crossings with additional branches of different angular momenta. For energies departing from zero, the main difference between panels a and b of Fig. 2 is that the energy branches are more densely spaced in Q2DM than QPM. This difference can be attributed to the small diffusivity  $s = 12.5$  nm used in the Q2DM. A smoother 1D kink is known to reduce the spacing of energy branches<sup>30,37</sup>.

In Fig. 3 we show the Q2DM energy spectra for different loop shapes as a function of their perimeters. Remarkably, the spectrum for noncircular loops show anticrossings of the branches. The square (b) shows an

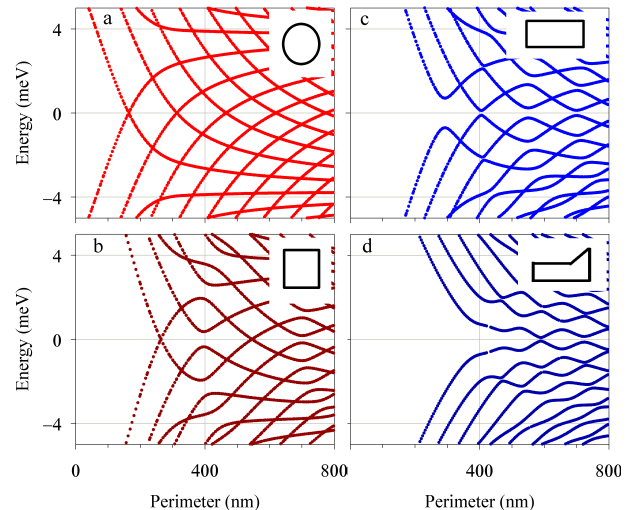


FIG. 3. Q2DM energy spectra as a function of perimeter for circle (a), square (b), rectangle (c) and irregular polygon (d). Parameters as in Fig. 2.

alternation of zero energy crossings and anticrossings as the perimeter increases. Both the rectangle (c) and the irregular polygon (d) show zero energy anticrossings in all cases, although the size of the anticrossing gap is not uniform. There is a general tendency for all shapes to decrease the anticrossing gaps for large perimeter, making the spectra shape independent in this limit.

The fact that, in addition to the circle, only the square shows crossings for some branches can be understood as a symmetry consequence. Inspired by the QPM, the branch crossing is possible in a square when, simultaneously, two conditions are fulfilled

$$\begin{cases} \mathcal{P} = n_1 \lambda_0, \\ e^{ik_0 L_x} = \pm i \Rightarrow \mathcal{P} = (2n_2 + 1)\lambda_0, \end{cases} \quad n_1, n_2 \in \mathbb{N}, \quad (7)$$

where  $k_0 = 2\pi/\lambda_0$  is the mode wavenumber. Only with  $n_1$  odd the crossing is then possible, as indeed obtained in Fig. 3b. The second condition in Eq. (7) corresponds to the requirement that a translation along the perimeter by the length of a side changes the state in a  $\pm i$  phase, which occurs when the total number of wavelengths to distribute in the four square sides is odd  $n_1 = 2n_2 + 1$ . In a rectangle one should replace  $L_x$  by  $L_x + L_y$  in this second condition, which then becomes not compatible with the first one and no crossing is therefore allowed. For the irregular shape (d), the lack of any symmetry is responsible for the absence of crossings in the spectrum.

We discuss next the results in presence of a magnetic field  $B$ . Figure 4 compares the analytic and numeric results for a circular loop when  $B = 0.5$  T. The magnetic field breaks the valley degeneracy of the loop eigenmodes, yielding asymmetric spectra with respect to energy inversion. We remark that Fig. 4 shows the results for a given valley. The results for the opposite valley, not shown, are

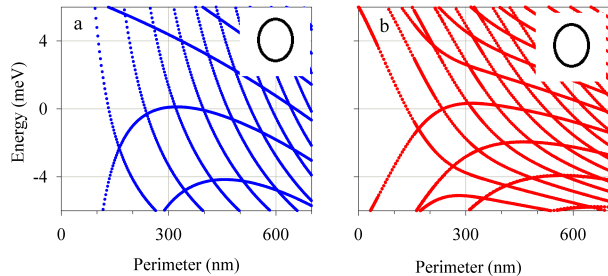


FIG. 4. Same as Fig. 2 with a finite magnetic field. Parameters: wall potential  $V_a = 10$  meV, smoothness  $s = 12.5$  nm and magnetic field  $B = 0.5$  T.

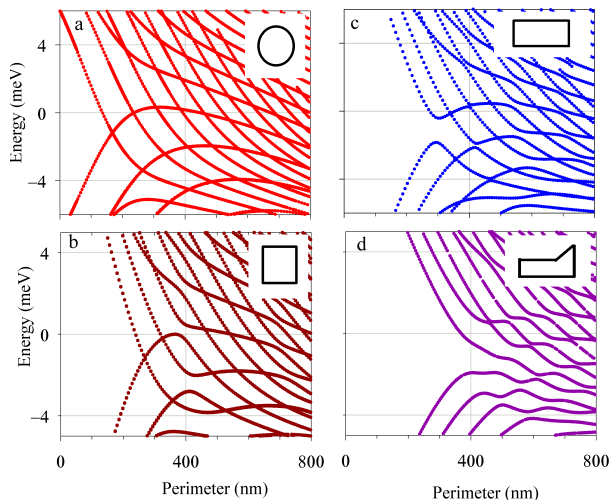


FIG. 5. Same as Fig. 3 with a finite magnetic field. Parameters as in Fig. 4.

shifted in the opposite direction restoring the symmetry of the spectrum for both energy and valley inversion ( $\mathcal{C}$  symmetry). There is again a good qualitative agreement between QPM and Q2DM, the most noticeable difference being the denser bunching of the energy branches within Q2DM, as in the  $B = 0$  cases discussed above.

In Fig. 5 we show the results of the 2D model at finite magnetic field for the different shapes. The field-induced asymmetry is similar when the geometrical structure changes. Branch anticrossings are present for nonsymmetric shapes, although they are not centered at zero energy but shifted vertically. Similarly to  $B = 0$  (cf. Fig. 3), we find that with an increase of the perimeter the shape-dependent features of the spectrum are washed out.

As a function of magnetic field, for a fixed loop dimension and shape, the loop spectrum shows a periodic behavior that is reminiscent of the Aharonov-Bohm effect. Figure 6 shows the result for a square in the QPM and Q2DM, both in good qualitative agreement. The en-

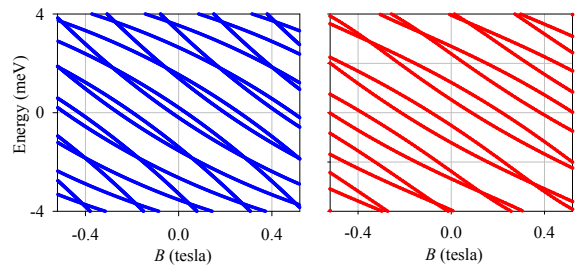


FIG. 6. Spectrum as a function of magnetic field for a square loop of a fixed perimeter in QPM (a) and Q2DM (b). Parameters: wall potential  $V_a = 10$  meV, smoothness  $s = 12.5$  nm and perimeter  $\mathcal{P} = 500$  nm.

ergy branches come in doublets, originating from the two kink branches  $f_{1,2}$  given by Eq. (1). The results in Fig. 6 are in general asymmetric with respect to energy inversion, in the same way as for the results as a function of perimeter (Fig. 5); the energy inversion symmetry being fulfilled at  $B = 0$  only. For different shapes the results show a similar periodicity, only that the field spacings between branch doublets must be scaled by the enclosed flux  $\Phi$ .

As with previous figures, the results of Fig. 6 are for a single valley; the energy branches for the reversed valley having the exactly opposite slope. The magnetic field slope of the branches is clearly indicating that the loop sustains persistent currents in finite fields, as discussed already for trivial and topological circular rings in Refs. 27 and 38, respectively. Hence, we investigate the shape dependence of the persistent current in topological loops as a possible probe of the geometric effects on topologically confined states. For definiteness, we focus on the current associated to the lowest positive-energy quasiparticle of the spectrum  $E_1$  from the derivative

$$J_1 = \frac{\partial E_1}{\partial B}. \quad (8)$$

The persistent current  $J_1$  for the different shapes is shown in Fig. 7 for a fixed perimeter of 500 nm. Due to the aforementioned valley and energy inversion symmetry, the persistent current has an odd symmetry with respect to field inversion, implying a vanishing value at zero field. The current is characterized by a sequence of alternating plateaus of almost constant values. This is an effect of the nearly linear dispersion of the energy levels with magnetic field. Positive and negative plateaus correspond to persistent currents of opposite valleys, circulating with opposed chiralities. Along the sequence from high symmetry (a, circle) to low symmetry (c rectangle and d irregular shapes) the behavior looks qualitatively similar, but the plateau lengths are reduced due to the increased number of field transitions. This is also expected since the flux  $\Phi$  is reduced for the deformed loops. Therefore, measuring the persistent current yields valuable information on the geometrical structure of the

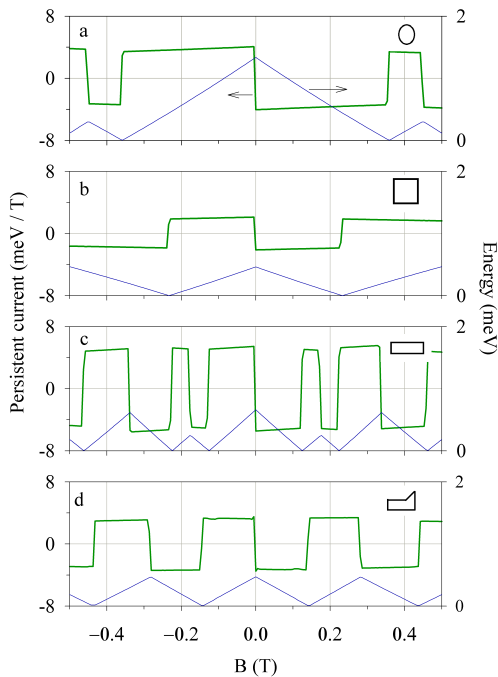


FIG. 7. Persistent current  $J_1$  (thick line, left scale) and energy  $E_1$  (thin line, right scale) of the lowest positive state as a function of the magnetic field for a fixed perimeter loop and the different shapes indicated in each panel. Parameters as in Fig. 6.

loop.

#### IV. CONCLUSIONS

We have investigated the confined states in topological loops built in bilayer graphene. We have devised an analytical model, the quantized perimeter model (QPM), based on the infinite straight kink, that provides the wavelength quantization along the loop perimeter. In addition, a full quantum 2D model (Q2DM), valid at low energies, has been numerically solved in order to ascertain the validity of the analytical model. A general good agreement between both models is found. For large sizes, the energy spectra are almost insensitive to the loop shape, as expected from QPM. For small sizes, we have found that Q2DM reflects shape dependence in the emergence of zero-energy crossings for circles, alternating crossings-anticrossings for squares, and only anticrossings for other more irregular structures. The magnetic field introduces energy-inversion asymmetries of the spectrum for a single valley and Aharonov-Bohm periodicities. Shape-dependent anticrossings in small loops are also present with magnetic fields. Finally, we have found that persistent currents are sensitive to shape-dependent features in presence of magnetic fields, which makes them a useful tool to look into bound states in topological sys-

tems.

Overall, our results are helpful for tailoring potential structures, finding the optimal geometry for possible applications in quantum computation with topological qubits or for valleytronic devices. Since there could be deviations from the intended symmetry due to fabrication limitations, our study emphasizes the importance of taking into account emerging spatial asymmetries for a careful characterization of the underlying physical system.

#### ACKNOWLEDGMENTS

We acknowledge support from AEI (Spain) Grant No. PID2020-117347GB-I00, MINECO/AEI/FEDER María de Maeztu Program for Units of Excellence MDM2017-0711.

#### Appendix A: Modeling

The Q2DM low energy Hamiltonian, Eq. (5), requires a specific spatial dependence of the asymmetric potential  $V_a(x, y)$ . This appendix contains the details of the modeling of different loop shapes with  $V_a(x, y)$  smooth profiles parameterized with a diffusivity  $s$ . The circle is described by a simple combination of logistic functions in the radial coordinate  $r = \sqrt{x^2 + y^2}$ ,

$$V_a^{(cir)}(r) = V_a^{(in)} \mathcal{F}(r; R_0, s) + V_a^{(out)} (1 - \mathcal{F}(r; R_0, s)), \quad (\text{A1})$$

where  $V_a^{(in,out)}$  are the constant values of asymmetric potential inside/outside of the loop and the logistic function reads

$$\mathcal{F}(r; R_0, s) = \frac{1}{1 + \exp[(r - R_0)/s]}. \quad (\text{A2})$$

To describe smooth square and rectangle shapes we first introduce the ranges of the Cartesian coordinates  $x \in [x_a, x_b]$ ,  $y \in [y_a, y_b]$  representing the loop inner area and then use a similar smooth parametrization in each Cartesian direction. Namely,

$$V_a^{(squ,rect)}(r) = V_a^{(in)} \mathcal{F}_{2D}(x, y) + V_a^{(out)} (1 - \mathcal{F}_{2D}(x, y)), \quad (\text{A3})$$

where

$$\mathcal{F}_{2D}(x, y) = (\mathcal{F}(x; x_b, s) - \mathcal{F}(x; x_a, s)) \times (\mathcal{F}(y; y_b, s) - \mathcal{F}(y; y_a, s)). \quad (\text{A4})$$

Finally, for the irregular shape we use the same modeling of Eq. (A3) but with the modification that  $y_b$  is no longer constant but the following piecewise function of  $x$

$$y_b(x) = \begin{cases} 0, & x < 0, \\ x y_b / x_b, & x > 0. \end{cases} \quad (\text{A5})$$

Notice that we assume centered positions of the loop, with  $x_{a,b} = \mp L_x/2$  and  $y_{a,b} = \mp L_y/2$ . For completeness, the perimeters for the different shapes are  $\mathcal{P}_{cir} = 2\pi R_0$ ,

$$\mathcal{P}_{squ} = 4L_x, \mathcal{P}_{rect} = 2(L_x + L_y), \mathcal{P}_{irr} = \frac{3}{2}(L_x + L_y) + \frac{1}{2}\sqrt{L_x^2 + L_y^2}.$$

- 
- <sup>1</sup> L. D. Landau and E. M. Lifshitz, *Quantum Mechanics (Non-Relativistic Theory)* (Butterworth-Heinemann, 1981) p. 29.
- <sup>2</sup> B. H. Bransden and C. J. Joachain, *Physics of Atoms and Molecules* (Pearson, 2006).
- <sup>3</sup> T. Ihn, *Semiconductor Nanostructures: Quantum states and electronic transport* (Oxford University Press, 2009).
- <sup>4</sup> Björn Trauzettel, Denis V. Bulaev, Daniel Loss, and Guido Burkard, “Spin qubits in graphene quantum dots,” *Nature Physics* **3**, 192–196 (2007).
- <sup>5</sup> J. Milton Pereira, P. Vasilopoulos, and F. M. Peeters, “Tunable quantum dots in bilayer graphene,” *Nano Letters* **7**, 946–949 (2007).
- <sup>6</sup> Patrik Recher, Johan Nilsson, Guido Burkard, and Björn Trauzettel, “Bound states and magnetic field induced valley splitting in gate-tunable graphene quantum dots,” *Phys. Rev. B* **79**, 085407 (2009).
- <sup>7</sup> Patrik Recher and Björn Trauzettel, “Quantum dots and spin qubits in graphene,” *Nanotechnology* **21**, 302001 (2010).
- <sup>8</sup> J. W. González, H. Santos, M. Pacheco, L. Chico, and L. Brey, “Electronic transport through bilayer graphene flakes,” *Phys. Rev. B* **81**, 195406 (2010).
- <sup>9</sup> J. W. González, H. Santos, E. Prada, L. Brey, and L. Chico, “Gate-controlled conductance through bilayer graphene ribbons,” *Phys. Rev. B* **83**, 205402 (2011).
- <sup>10</sup> P. A. Orellana, L. Rosales, L. Chico, and M. Pacheco, “Spin-polarized electrons in bilayer graphene ribbons,” *Journal of Applied Physics* **113**, 213710 (2013), <https://doi.org/10.1063/1.4809752>.
- <sup>11</sup> D.R. da Costa, M. Zarenia, Andrey Chaves, G.A. Farias, and F.M. Peeters, “Analytical study of the energy levels in bilayer graphene quantum dots,” *Carbon* **78**, 392–400 (2014).
- <sup>12</sup> Marius Eich, F. Herman, Riccardo Pisoni, Hiske Overweg, Annika Kurzmann, Yongjin Lee, Peter Rickhaus, Kenji Watanabe, Takashi Taniguchi, Manfred Sigrist, Thomas Ihn, and Klaus Ensslin, “Spin and valley states in gate-defined bilayer graphene quantum dots,” *Phys. Rev. X* **8**, 031023 (2018).
- <sup>13</sup> Annika Kurzmann, Hiske Overweg, Marius Eich, Alessia Pally, Peter Rickhaus, Riccardo Pisoni, Yongjin Lee, Kenji Watanabe, Takashi Taniguchi, Thomas Ihn, and Klaus Ensslin, “Charge detection in gate-defined bilayer graphene quantum dots,” *Nano Letters* **19**, 5216–5221 (2019).
- <sup>14</sup> V. Clericò, J. A. Delgado-Notario, M. Saiz-Bretín, A. V. Malyshev, Y. M. Meziani, P. Hidalgo, B. Méndez, M. Amado, F. Domínguez-Adame, and E. Diez, “Quantum nanoconstrictions fabricated by cryo-etching in encapsulated graphene,” *Sci. Rep.* **9**, 13572 (2019).
- <sup>15</sup> L. Banszerus, A. Rothstein, T. Fabian, S. Möller, E. Icking, S. Trellenkamp, F. Lentz, D. Neumaier, K. Watanabe, T. Taniguchi, F. Libisch, C. Volk, and C. Stampfer, “Electron hole crossover in gate-controlled bilayer graphene quantum dots,” *Nano Letters* **20**, 7709–7715 (2020).
- <sup>16</sup> L. Banszerus, K. Hecker, E. Icking, S. Trellenkamp, F. Lentz, D. Neumaier, K. Watanabe, T. Taniguchi, C. Volk, and C. Stampfer, “Pulsed-gate spectroscopy of single-electron spin states in bilayer graphene quantum dots,” *Phys. Rev. B* **103**, L081404 (2021).
- <sup>17</sup> Hongki Min, J. E. Hill, N. A. Sinitsyn, B. R. Sahu, Leonard Kleinman, and A. H. MacDonald, “Intrinsic and rashba spin-orbit interactions in graphene sheets,” *Phys. Rev. B* **74**, 165310 (2006).
- <sup>18</sup> Yugui Yao, Fei Ye, Xiao-Liang Qi, Shou-Cheng Zhang, and Zhong Fang, “Spin-orbit gap of graphene: First-principles calculations,” *Phys. Rev. B* **75**, 041401 (2007).
- <sup>19</sup> M. Gmitra, S. Konschuh, C. Ertler, C. Ambrosch-Draxl, and J. Fabian, “Band-structure topologies of graphene: Spin-orbit coupling effects from first principles,” *Phys. Rev. B* **80**, 235431 (2009).
- <sup>20</sup> Mengqiao Sui, Guorui Chen, Ligu Ma, Wen-Yu Shan, Dai Tian, Kenji Watanabe, Takashi Taniguchi, Xiaofeng Jin, Wang Yao, Di Xiao, and Yuanbo Zhang, “Gate-tunable topological valley transport in bilayer graphene,” *Nature Physics* **11**, 1027–1031 (2015).
- <sup>21</sup> Hiske Overweg, Angelika Knothe, Thomas Fabian, Lukas Linhart, Peter Rickhaus, Lucien Wernli, Kenji Watanabe, Takashi Taniguchi, David Sánchez, Joachim Burgdörfer, Florian Libisch, Vladimir I. Fal’ko, Klaus Ensslin, and Thomas Ihn, “Topologically nontrivial valley states in bilayer graphene quantum point contacts,” *Phys. Rev. Lett.* **121**, 257702 (2018).
- <sup>22</sup> R. Kraft, I. V. Krainov, V. Gall, A. P. Dmitriev, R. Krupke, I. V. Gornyi, and R. Danneau, “Valley subband splitting in bilayer graphene quantum point contacts,” *Phys. Rev. Lett.* **121**, 257703 (2018).
- <sup>23</sup> Ivar Martin, Ya. M. Blanter, and A. F. Morpurgo, “Topological confinement in bilayer graphene,” *Phys. Rev. Lett.* **100**, 036804 (2008).
- <sup>24</sup> C. L. Kane and E. J. Mele, “Quantum spin hall effect in graphene,” *Phys. Rev. Lett.* **95**, 226801 (2005).
- <sup>25</sup> B. A. Bernevig, T. L. Hughes, and S.-C. Zhang, “Quantum spin hall effect and topological phase transition in hgte quantum wells,” *Science* **314**, 1757 (2006).
- <sup>26</sup> M. König, S. Wiedmann, C. Brüne, A. Roth, H. Buhmann, L. W. Molenkamp, X.-L. Qi, and S.-C. Zhang, “Quantum spin hall insulator state in hgte quantum wells,” *Science* **318**, 766 (2007).
- <sup>27</sup> L. J. P. Xavier, J. M. Pereira, Andrey Chaves, G. A. Farias, and F. M. Peeters, “Topological confinement in graphene bilayer quantum rings,” *Applied Physics Letters* **96**, 212108 (2010).
- <sup>28</sup> Edward McCann and Mikito Koshino, “The electronic properties of bilayer graphene,” *Reports on Progress in Physics* **76**, 056503 (2013).
- <sup>29</sup> A.V. Rozhkov, A.O. Sboychakov, A.L. Rakhmanov, and Franco Nori, “Electronic properties of graphene-based bilayer systems,” *Physics Reports* **648**, 1–104 (2016), electronic properties of graphene-based bilayer systems.
- <sup>30</sup> Nassima Benchtaber, David Sánchez, and Llorenç Serra, “Scattering of topological kink-antikink states in bilayer graphene,” (2021), arXiv:2103.13323 [cond-mat.mes-hall].

- <sup>31</sup> Jing Li, Ke Wang, Kenton J. McFaul, Zachary Zern, Yafei Ren, Kenji Watanabe, Takashi Taniguchi, Zhenhua Qiao, and Jun Zhu, “Gate-controlled topological conducting channels in bilayer graphene,” *Nature Nanotechnology* **11**, 1060–1065 (2016).
- <sup>32</sup> H. Chen, P. Zhou, J. Liu, J. Qiao, B. Oezylmaz, and J. Martin, “Gate controlled valley polarizer in bilayer graphene,” *Nature Communications* **11**, 1202 (2020).
- <sup>33</sup> R. B. Lehoucq, D. C. Sorensen, and C. Yang, *ARPACK Users Guide: Solution of Large-Scale Eigenvalue Problems with Implicitly Restarted Arnoldi Methods* (Philadelphia: SIAM. ISBN 978-0-89871-407-4, 1998).
- <sup>34</sup> Leonard Susskind, “Lattice fermions,” *Phys. Rev. D* **16**, 3031–3039 (1977).
- <sup>35</sup> H.B. Nielsen and M. Ninomiya, “Absence of neutrinos on a lattice: (i). proof by homotopy theory,” *Nuclear Physics B* **185**, 20–40 (1981).
- <sup>36</sup> Alexis R. Hernández and Caio H. Lewenkopf, “Finite-difference method for transport of two-dimensional massless Dirac fermions in a ribbon geometry,” *Phys. Rev. B* **86**, 155439 (2012).
- <sup>37</sup> M. Zarenia, J. M. Pereira, G. A. Farias, and F. M. Peeters, “Chiral states in bilayer graphene: Magnetic field dependence and gap opening,” *Phys. Rev. B* **84**, 125451 (2011).
- <sup>38</sup> P. Recher, B. Trauzettel, A. Rycerz, Ya. M. Blanter, C. W. J. Beenakker, and A. F. Morpurgo, “Aharonov-Bohm effect and broken valley degeneracy in graphene rings,” *Phys. Rev. B* **76**, 235404 (2007).